ACS APPLIED MATERIALS & INTERFACES

www.acsami.org

Research Article

Overcoming Stability and Substrate Adhesion Challenges by Laser-Induced Transfer of MXenes

Anna Lipovka,* Raul D. Rodriguez,* Aura Garcia, Dmitry Kogolev, Ziyang Song, Ranran Wang,* and Evgeniya Sheremet

Cite This: https://doi.org/10.1021/acsami.5c18259

Read Online

ACCESS | Metrics & More | Article Recommendations | Supporting Information

ABSTRACT: Despite their metallic conductivity and solution processability, the practical application of MXenes is limited by two persistent challenges: poor adhesion to substrates and low chemical stability in air, which leads to oxidation. Conventional stabilization approaches often involve antioxidant doping or polymer lamination that may compromise electrical conductivity. Here, we tackle these issues by introducing a single-step laser-induced transfer (LIT) process that engineers the MXene-substrate interface to enhance adhesion and chemical stability simultaneously. Our method exploits the spatial confinement of MXene films sandwiched between a glass slide and a polymer substrate. This configuration creates an oxygen-depleted microenvironment, and under laser irradiation allowing for the simultaneous transfer of $Ti_3C_2T_x$ MXene films onto both top and bottom substrates. LIT results in solid-state sintering that, in addition to boosting adhesion, also provides protective effects due to the development of a carbon-rich surface layer. This enhanced adhesion and stability are demonstrated by low sheet resistance, remaining below 25 Ω/sq for MXenes/glass and below 6 Ω/sq for MXenes/TPU after environmental aging for 10 days at 95 ± 2% relative humidity and 40−60 °C. In contrast, conventional direct laser patterning fails to achieve this level of robustness and instead accelerates MXenes decomposition. The suppressed oxidation and mechanical stability enabled by LIT allowed the creation of robust interfaces suitable for electrothermal heaters and proof-of-concept breath sensors. This work establishes laser processing not merely as a patterning tool but also as a powerful interfacial engineering technique, resolving key issues that affect MXene implementation in electronics, sensors, and wearable devices.

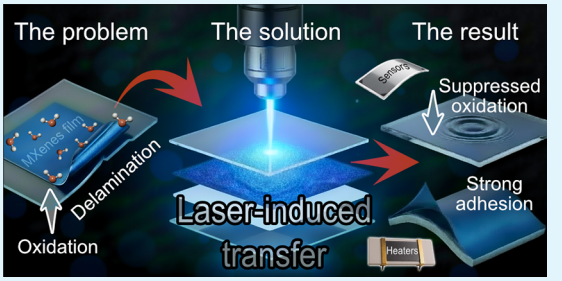

KEYWORDS: *MXenes, 2D Materials, Laser Processing, Laser-Induced Transfer (LIT), Laser-Induced Backward Transfer (LIBT), Laser-Induced Forward Transfer (LIFT), Adhesion*

1. INTRODUCTION

Emerging two-dimensional (2D) materials are shaping the future of advanced electronics, sensors, and the Internet of Things. Take, for instance, MXenes. These 2D transition metal carbides and nitrides are known for their remarkable combination of high metal-like conductivity (up to 24,000 S/cm),[1] driven by a high electron density at the Fermi level. Their intrinsic hydrophilicity, resulting from tunable surface functional groups such as −OH, −O−, and −F, also plays a crucial role in their applications,[2,3] enabling solution processing and the straightforward fabrication of conductive films on various substrates. Therefore, MXenes are considered promising materials for high-performance flexible electronics[2−4] and catalysis.[5]

Despite this potential, the transition from lab-scale demonstrations to commercially available functional electronics is limited by two challenges: (1) poor adhesion of MXene films to hydrophobic substrates (e.g., some commonly used polymers),[6] and (2) rapid degradation of electrical and mechanical properties under ambient conditions.[7]

Weak interfacial adhesion results in nonuniform films, gradual degradation, and delamination, which ultimately lead to device failure. Various strategies have been reported to mitigate these issues, including oxygen plasma surface pretreatment,[8] surfactant addition, or the salt-assisted assembly method.[9] However, these solutions often compromise conductivity, introduce contaminants, and lack universal applicability across different substrates.

Conductivity loss and robustness issues due to the irreversible oxidation and mechanical delamination of MXene films in humid or heated environments[2,10] have been partly addressed through postprocessing techniques such as antioxidant doping, thermal annealing, and surface coating.[11] A

Received: September 12, 2025
Revised: November 11, 2025
Accepted: November 18, 2025

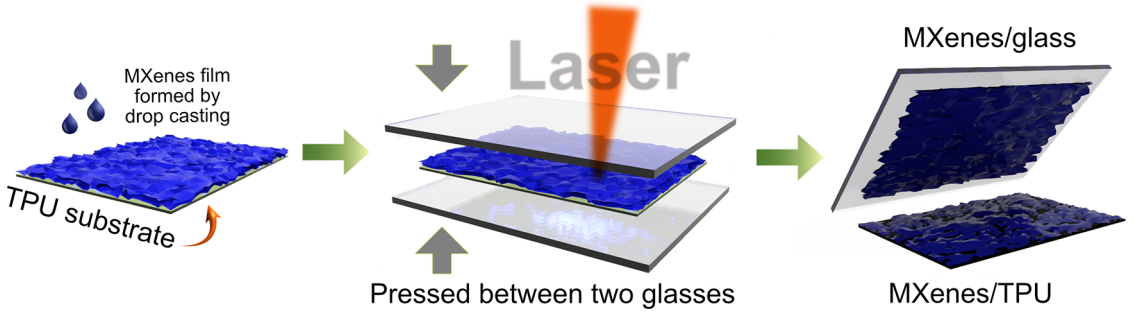

Figure 1. Schematic representation of the laser-assisted MXene transfer process. The illustration shows: 1) Deposition of a $Ti_3C_2T_x$ MXene film via drop-casting onto a TPU substrate, 2) Pressing MXenes-coated TPU between two transparent glass slides, and 3) Laser processing through the top glass. The two resulting interfaces demonstrate enhanced adhesion, as observed for 4) MXenes/glass and 5) MXenes/TPU sides.

recent development involves protecting MXenes with thin polymer film lamination, which has effectively extended their application in triboelectric nanogenerators.[12] However, these methods often involve complex multistep processes and do not create a robust, covalent-like MXene-substrate interface necessary to resist both delamination and environmental degradation.

Laser processing is currently revolutionizing nanomaterial modification, offering a transformative solution to both adhesion and stability challenges in a single step.[13] It allows achieving tremendous results for stable, conductive, and high-resolution patterning with the whole range of materials from graphene[14] to liquid metals.[15] However, in the case of MXenes, its application has been narrowly focused on patterning for supercapacitors.[16] Recent studies have introduced laser-induced MXene-based composites for electronic applications. For instance, Li et al. developed a MXene/graphene composite by mixing it with polyamide acid as a precursor for graphene to fabricate an efficient pressure sensor.[17] Another method involved depositing MXenes onto a polyimide film via spin-coating, followed by direct laser irradiation.[18] Additionally, laser-directed bubble printing has been used to pattern MXene-semiconductor composites on glass slides; however, the stability issues of MXenes have resulted in significant degradation of device performance over time due to air exposure.[19]

Here, we reframe laser processing not as a patterning tool, but as an interface engineering strategy aimed at enhancing the adhesion of MXenes to both rigid (glass) and flexible (thermoplastic polyurethane, TPU) substrates. This results in robust MXenes-substrate interfaces and extends device operation. Our method requires no pre- or post-treatment and applies even to aged MXene films synthesized over a year ago.

To address the issue of conventional laser processing, which accelerates oxidative decomposition due to high temperatures in air, we introduce a sandwich-like configuration that creates a closed, oxygen-depleted microenvironment in ambient conditions. We propose mechanisms that enhance adhesion and provide robust electrical conductivity under harsh conditions, including high humidity and high temperatures. Furthermore, we demonstrate the applicability of our MXene-based structures in electrothermal heaters and breath sensors, opening new opportunities to create high-performance, long-lasting MXene electronics.

2. RESULTS AND DISCUSSION

2.1. Laser-Induced Transfer. $Ti_3C_2T_x$ is currently the most widely used MXene, synthesized by selective etching of the Ti_3AlC_2 MAX phase (see details in Experimental Section). For deposition onto TPU substrates, it was diluted to form an aqueous dispersion. Initially, the $Ti_3C_2T_x$ surface is covered by Ti(II) and Ti(III) suboxides, but tends to fully oxidize to Ti(IV) over time.[20] Thus, to replicate real-world conditions and enhance the practical relevance of our findings, dried MXene films on TPU were further stored untouched in sealed bags for one year without any intervention. After this extended storage period, the absence of adhesion-enhancing procedures resulted in the MXene films being loosely attached to the TPU substrates, becoming nearly free-standing (see Figure S1). Despite this, the samples maintained high electrical conductivity, with sheet resistance values in the ~0.5−2 Ω/sq range, indicating potential for electronic applications. However, the poor interfacial adhesion significantly compromises reliability due to the need for film immobilization and electrical contacting, which are crucial for device fabrication.

In most reported cases, direct laser irradiation of MXenes in air accelerates surface oxidation, sometimes even intentionally.[17,21,22] Our initial findings confirmed these results, as direct patterning with a green laser led to significant oxidation of $Ti_3C_2T_x$ to TiO_2, as demonstrated by Raman spectroscopy (Note S1 and Figure S2). To enhance adhesion while preserving the electrical conductivity and original properties of MXenes, we aimed to minimize additional oxidation, which required avoiding direct laser patterning. Instead, we adapted Laser-Induced Transfer (LIT) as an effective approach to achieve all of our objectives. Figure 1 shows a schematic representation of the experimental configuration, which effectively mitigates oxidation risk during processing by creating localized oxygen-depleted conditions without the need for an inert atmosphere or vacuum conditions. This design was inspired by our previous work on the simultaneous reduction and backward transfer of graphene oxide onto glass.[23] In this study, we hypothesized that a single-step LIT process could enable MXenes to adhere to both the top and bottom substrates, enhancing mechanical stability beyond what conventional surface pretreatments or direct patterning can achieve.

In this LIT setup, laser irradiation at a wavelength of 436 nm was directed through the top transparent glass and absorbed by the dark MXenes film surface deposited on TPU, triggering localized high-temperature processing. The active surfaces in this case were the top glass and TPU substrate. After laser

https://doi.org/10.1021/acsami.5c18259
ACS Appl. Mater. Interfaces XXXX, XXX, XXX−XXX

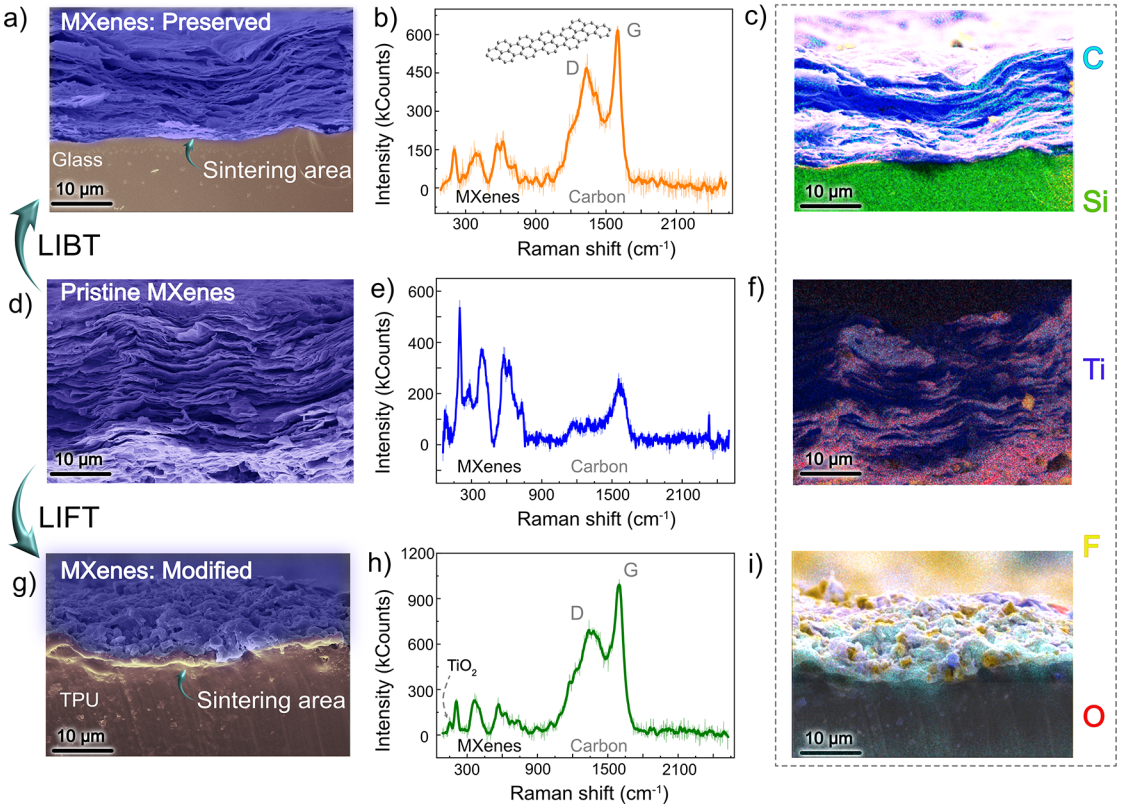

Figure 2. Characterization and comparison of original $Ti_3C_2T_x$ and after laser transfer to glass and TPU substrates. SEM cross-sectional images, Raman spectra, and EDX cross-sectional maps for: a,b,c) MXenes/glass; d,e,f) pristine MXenes; and g,h,i) MXenes/TPU.

processing, the sandwich structure was separated, resulting in MXenes being transferred to both contact surfaces, thereby forming robust interfaces with them. This approach is conceptually related to the recently reported laser bidirectional printing technique by Li et al., where laser irradiation facilitated simultaneous synthesis and transfer of graphene onto two substrates via a photothermal and plasma-induced process.[24] Unlike that work, which relies on in situ carbonization of the precursor, our method goes beyond film transferring with laser-induced graphene formation but instead employs presynthesized MXene films for interface engineering.

In our case, laser irradiation induced the adhesion of MXenes to the top glass via Laser-Induced Backward Transfer (LIBT) and simultaneously to the TPU substrate by Laser-Induced Forward Transfer (LIFT). The materials obtained are denoted as MXenes/glass and MXenes/TPU, respectively. We experimentally determined that the working region for efficient transfer for the blue laser is 320−400 mJ and a pulse duration of 300−350 μs (see Note S2 and Figure S3). Shifting out of this range either fails to initiate LIBT or results in the materials burning.

2.2. MXenes/Glass and MXenes/TPU. The synthesized $Ti_3C_2T_x$ exhibits a typical layered structure for MXenes (Figure 2d). Energy-Dispersive X-ray spectroscopy (EDX) analysis confirms a uniform distribution of titanium and carbon throughout the sample (Figure 2f). However, the bottom side, which is in contact with the TPU surface, accumulates more fluorine from the precursor, likely due to the sedimentation of heavy fluorine-containing crystals during the film drying process. This resulted in morphological and elemental differences between the top and bottom surfaces of the MXenes (see Note S3 and Figure S4).

During laser processing, the radiation passes through the top glass surface and is absorbed directly by the MXenes film on TPU, where it is converted into heat. The multilayered $Ti_3C_2T_x$, having excellent thermal conductivity,[25] efficiently dissipates this heat, resulting in intense gas release within the closed system. This photothermal effect is the driving force behind the separation of MXene layers and their transfer (LIBT and LIFT) toward the glass and polymer substrates.

Most MXene layers transfer to the upper glass surface via LIBT without damage or delamination. Cross-sectional SEM imaging reveals a reduction in the interlayer spacing compared to pristine MXenes (Figure 2a and 2d), which is in contrast with the case of graphene oxide, where LIBT increased the roughness of reduced graphene oxide/glass.[23] We attribute the spacing reduction to interlayer water deintercalation and removal of terminal groups during the rapid heating, as shown previously with thermal annealing.[26,27] It has recently been shown that $Ti_3C_2T_x$ under vacuum annealing at 600 °C, results in the complete removal of water.[10] This high temperature can be reached in our configuration through photothermal heating.[23] Additionally, laser processing under pressure may further contribute to compaction. Once the first MXene layer adheres to the glass surface, subsequent layers stack with reduced spacing, allowing the glass to absorb heat directly. This change in spacing contributes to the mechanical robustness and well-preserved MXenes morphology of the MXenes/glass interface.

Initially, we expected that the high temperatures generated during laser processing would cause the substrate to melt and intermix with MXenes during cooling, similar to what occurs with graphene. However, cross-sectional SEM and EDX images (Figures 2a and 2c) show no evidence of these effects. Instead,

https://doi.org/10.1021/acsami.5c18259
ACS Appl. Mater. Interfaces XXXX, XXX, XXX−XXX

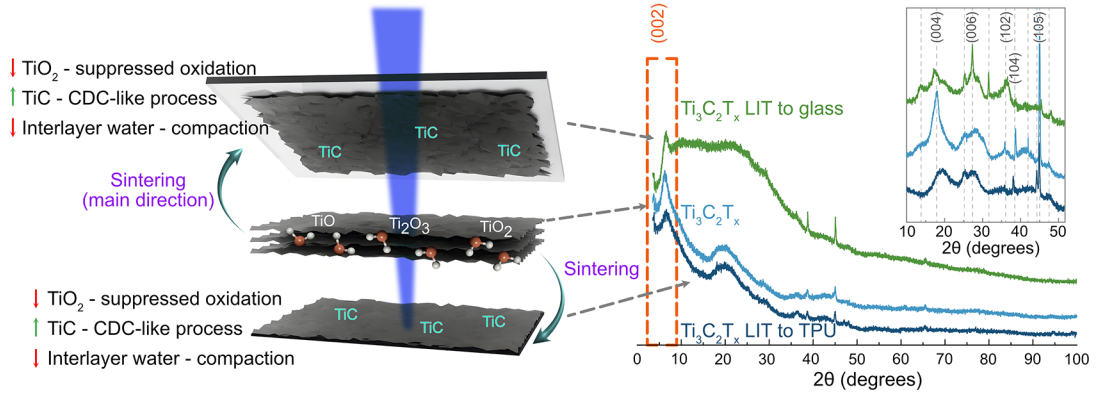

Figure 3. Schematic illustration of the processes taking place during LIBT and LIFT, and XRD patterns of pristine MXenes, MXenes/glass, and MXenes/TPU.

the characterization reveals a clear and intact boundary between the MXene layers and the glass substrate, ruling out a liquid-phase mechanism. These findings are consistent with a solid-state sintering process, where materials bond and densify into a solid mass through the application of heat below their melting point.[28,29] The external pressure applied in the LIT system enhances densification, while the oxygen-depleted environment reduces oxidation, which will be discussed further. As the MXene layers reach the glass substrate, localized heating promotes solid-state sintering at the interface, ensuring strong adhesion that can withstand mechanical stress and washing.

MXenes adhere to TPU in a manner similar to glass, forming an MXenes/TPU interface through laser sintering. However, the MXenes/TPU surface differs significantly from the MXenes/glass, as shown in the SEM cross-sectional image (Figure 2g). Our LIT configuration ensures that, regardless of the substrate, for instance, if the TPU substrate is replaced with glass at the bottom, the most efficient transfer occurs from LIBT to the top glass interface (Figure S5). This preferential transfer direction is likely due to gas release during laser processing, which pushes loosely bonded layers upward and prevents TPU melting, as is the case when TPU is the top substrate (Figure S5). Although LIFT is more commonly used, it tends to cause more structural disruption and defects than LIBT. Consequently, the bottom surface of the MXenes film is more defective, resulting in a less preserved MXenes structure on MXenes/TPU and reduced transfer to the TPU substrate. Nonetheless, EDX mapping confirms the presence of Ti and C, and the Raman spectrum shows that MXenes were partially preserved in MXenes/TPU (Figures 2h and 2i).

Raman spectroscopy analysis of MXenes/glass and MXenes/TPU after laser processing (Figures 2b and 2h) indicates three crucial points. First, both interfaces show similar spectra with the characteristic one of $Ti_3C_2T_x$ (Figure 2e).[30] The A_{1g} mode at ~200 cm^{-1} corresponds to out-of-plane vibrations of Ti and C atoms, as well as surface groups, while the band at ~400 cm^{-1} represents E_g in-plane vibrations of surface groups attached to Ti. The broad region with a distinguishable peak at ~600 cm^{-1} is attributed to vibrations of C atoms (E_g and A_{1g}).[31] This indicates that despite the high temperatures and morphological changes, laser processing preserves the original MXenes structure.

Second, the MXenes/glass interface shows no detectable TiO_2 anatase phase (~140 cm^{-1}), while the MXenes/TPU in some cases exhibits a weak signal. The observation of this mode indicates oxidative decomposition of MXenes, and its absence shows that the LIT oxygen-depleted microenvironment results in minimal MXene oxidation. In this tightly confined sandwich configuration, the intense photothermal heating instantly vaporizes water molecules, resulting in high localized pressure that forces out all air, including oxygen, preventing the oxidation of MXenes. Maintaining such low oxidation levels is not possible with direct laser patterning in air (Note S1), highlighting one of the key benefits of our transfer method.

Finally, both interfaces reveal prominent D and G carbon peaks. The original MXenes also demonstrate the presence of carbon originating from their structure; however, the intensity and shape of the peaks significantly change after LIT, indicating carbonization. The sharp G peak originates from sp^2-hybridized carbon structures, caused by the presence of graphitic domains, while the broad D peak arises from defect-induced vibrations in disordered carbon. These peaks are not derived from the substrates but are likely due to partial carbon extraction from the carbide structure, caused by vacancy-mediated carbon rearrangement during high-temperature photothermal processing, and resulting in partial carbide-derived carbon formation (CDC).

X-ray diffraction (XRD) patterns of the original MXenes indicates the most characteristic MXene peak at 6.5° attributed to (002) plane, as well as distinctive peaks at 17.7°, 27.4°, 36.2°, 38.1°, 45.1°, and 60.5° correlated to the (004), (006), (102), (104), (105), and (110) indices, respectively. The patterns were achieved through two independent analyses, confirming the successful synthesis of MXenes from the MAX phase,[32] and preservation of MXene structure at both MXenes/glass and MXenes/TPU interfaces (Figure 3).

Both LIBT and LIFT processes yielded MXene-rich surfaces with significantly enhanced adhesion to glass and polymer, retaining their structure after rinsing with water or undergoing peel-off tests with adhesive tape (Figure S6). These results support our hypothesis on the capability of laser processing to create durable MXene-substrate interfaces suitable for practical applications.

2.3. Surface State of MXenes-Based Interfaces. The performance of electronic devices based on MXenes/glass and MXenes/TPU interfaces is significantly affected by their surface chemistry, which determines the properties of the active layer. Our findings and proposed mechanisms are summarized in Figure 3. We employed X-ray photoelectron

https://doi.org/10.1021/acsami.5c18259
ACS Appl. Mater. Interfaces XXXX, XXX, XXX−XXX

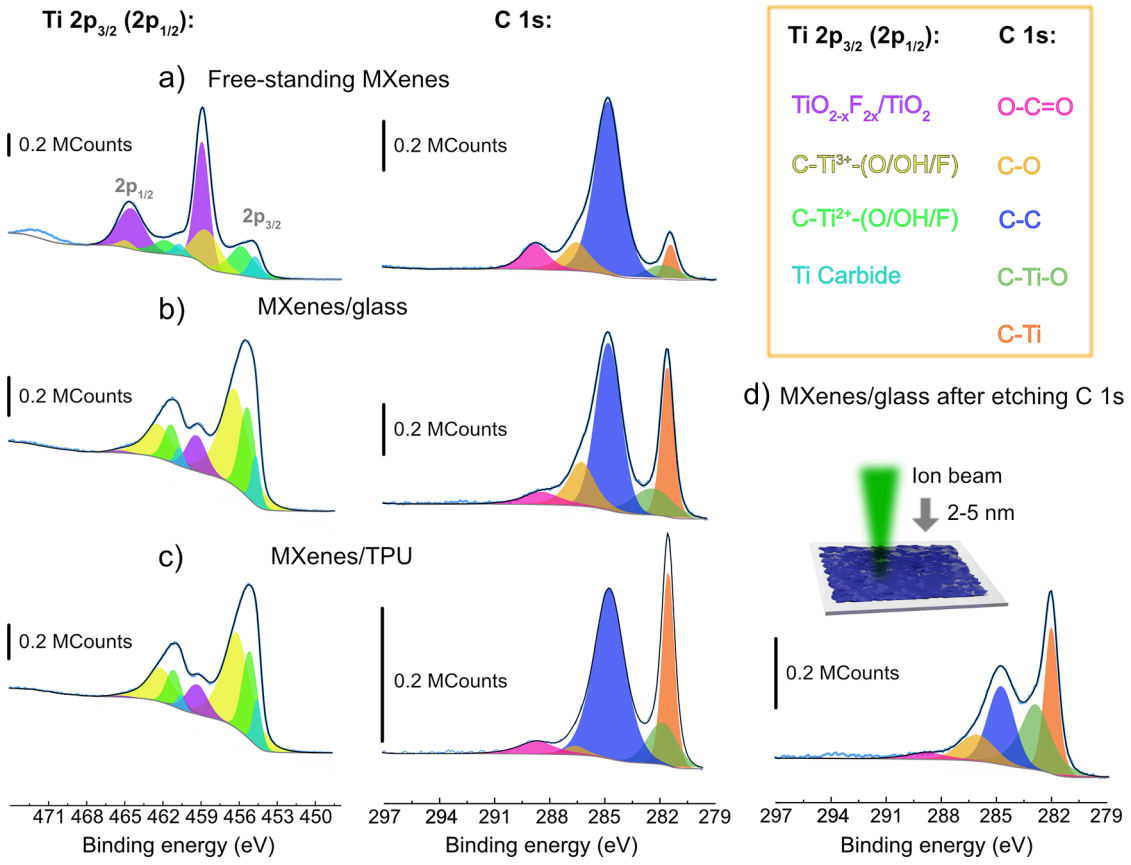

Figure 4. XPS analysis of the surface state of $Ti_3C_2T_x$ and their laser-induced interfaces with glass and TPU. Ti 2p and C 1s narrow regions of a) free-standing MXenes, b) MXenes/glass interface formed by LIBT, and c) MXenes/TPU interface formed by LIFT. d) MXenes/glass after etching several nanometers.

spectroscopy (XPS) as a key analytical tool to analyze the surface state and oxidation behavior.

The critical range for analysis is the Ti 2p narrow region represented by the Ti $2p_{3/2}$ and Ti $2p_{1/2}$ peaks, which should ideally maintain a 2:1 ratio. This region is characterized by three distinct peaks (along with associated satellites), indicative of titanium oxides: TiO (Ti^{2+}), Ti_2O_3 (Ti^{3+}), and TiO_2 (Ti^{4+}), and one of titanium carbide (also with a satellite). When $Ti_3C_2T_x$ MXenes oxidize, they predominantly form TiO_2, indicated by a characteristic peak around 459−459.5 eV. We compared the Ti 2p spectra of original free-standing $Ti_3C_2T_x$ (Figure 4a), MXenes/glass (Figure 4b), and MXenes/TPU (Figure 4c). The analysis demonstrates that LIT fundamentally changes MXene oxidation pathways. The top layer of original MXenes is initially oxidized, having an intense TiO_2 peak. Crucially, after laser sintering, both MXenes/glass and MXenes/TPU exhibited a significant decrease in the intensity of peaks related to the TiO_2 phase, meaning that LIT could be used as an approach to "prolong MXenes' life" regardless of their original oxidation state. This result is attributed to the rearrangement of carbon atoms during laser processing, which correlates with the increase in the TiC component (~454.7 eV for $2p_{3/2}$ and ~460.8 eV for $2p_{1/2}$), and supports the notion of heat-induced removal of terminal groups and intercalated water. These critical findings show that although MXene oxidation is unavoidable, laser sintering in our configuration not only enhances adhesion and structural robustness but also suppresses surface oxidation, thereby preserving the structure and conductivity of the original MXenes.

Details of the laser-induced changes are evident in the C 1s narrow region. After the LIBT process, the TiC band intensity (~281.5 eV) increased in MXenes/glass, as shown in Figures 4a and 4b, indicating the strengthening of carbide bonds and higher carbon content. Similar results were observed for MXenes/TPU (Figure 4c).

To investigate the structure beneath the topmost layers of MXenes/glass, we performed localized etching to remove several nanometers of material from the surface (Figure 4d). Remarkably, the carbide band intensity exhibited minimal reduction and remained more pronounced than in the original MXenes. In contrast, the C−C bond (~285 eV) decreased significantly, while the C−Ti−O (~282.5 eV) increased, suggesting that the CDC-like process selectively affects the surface region at the cleavage point. These are the interfaces created when the glass-MXenes-TPU sandwich gets opened, which occurs in regions with the highest graphitization.

This interpretation is supported by Raman spectroscopy results (Figures 2b, 2e, and 2h), which show that laser irradiation promotes CDC-initiated carbonization, resulting in a sp^2-hybridized, disordered carbon phase at the newly formed MXene-composite interface. Etching in XPS experiments removed the top carbonized layers, exposing the underlying C−Ti−O bonds. Additionally, the high-energy etching may have contributed to bond rearrangements, increasing the C−Ti−O bond while reducing the signal from the C−C bond. This suggests that laser processing not only modifies the surface chemistry but also reinforces the stability of the underlying structure in the form of TiC. The Ti 2p narrow

https://doi.org/10.1021/acsami.5c18259
ACS Appl. Mater. Interfaces XXXX, XXX, XXX−XXX

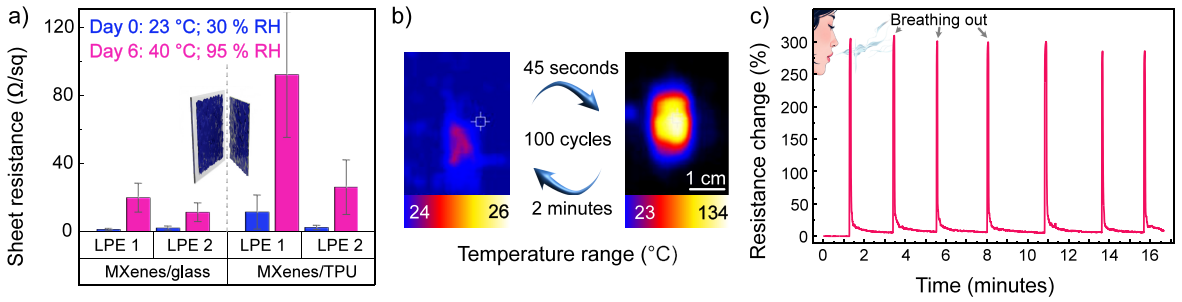

Figure 5. a) Sheet resistance of MXenes/glass and MXenes/TPU interfaces and its change after a week in an environmental chamber and additional immersion for 1 day in boiling water. b) Performance of MXenes/glass as an electrothermal heater, demonstrating uniform heat distribution and thermal stability. c) MXenes/PET proof-of-concept breath sensor.

region showed no significant changes after etching (Figure S7). The analysis of survey spectra of pristine MXenes and their interfaces revealed significant changes in the C/O ratios, supporting our conclusions from the narrow regions characterization. Notably, the C/O ratio increased for MXenes/glass and MXenes/TPU, confirming that the carbonization of the top surface was induced by laser processing (See Table S1). Etching of MXenes/glass exposed underlying layers with suboxides, restoring the C/O ratio closer to that of unprocessed $Ti_3C_2T_x$. Thus, LIT preserved MXenes' structure, eliminated interfacial water, and created carbon-based "bridges" to enhance adhesion and reduce oxidation.

To optimize the LIT process and validate the proposed mechanism, we systematically investigated the effects of laser parameters on transfer within the established working range (Note S2). In addition to enhancing MXenes' adhesion to the polymer side, we pretreated the TPU substrates with plasma before MXene deposition, which is a standard approach for improving wettability and bonding. In Table S2 of the Supporting Information, we present a comparative analysis within this range, including assessments of interface morphology (cross-sectional SEM), surface morphology (optical microscopy), TiC content and C/O ratio (XPS), and suppressed oxidation (XPS Ti 2p and Raman spectroscopy). We confirmed that changes in laser parameters within the working range have an insignificant impact on both MXenes/glass and MXenes/TPU interfaces. However, plasma pretreatment promoted adhesion and transfer to the polymer side, resulting in 40−70 μm thick MXenes/TPU interfaces (compared to ∼38.5 μm for pristine MXenes on TPU). Across all parameters, LIT consistently led to suppressed oxidation (decrease in TiO_2 band intensity compared to original MXenes), a consistent rise in TiC content (as evident in C 1s narrow region), and carbonization (higher C/O ratios of 2.39 ± 0.06 for MXenes/glass and 2.11 ± 0.09 for MXenes/TPU versus 0.96 ± 0.04 for pristine MXenes). Still, in all cases, there is no evidence of composite formation, and these outcomes support the proposed mechanisms of solid-state sintering and CDC-initiated carbonization in an oxygen-depleted microenvironment.

2.4. Maintaining High Electrical Conductivity and Interfacial Adhesion. To evaluate the reliability of our interfaces in real-world conditions, we conducted two complementary environmental aging tests, monitoring sheet resistance as detailed in the Experimental Section.

In the first test, we evaluated the long-term stability of MXenes/glass and MXenes/TPU interfaces, including those derived from plasma-treated TPU substrates before MXene deposition (as discussed in Table S2). We also included a set of reference samples: MXenes deposited directly on glass, untreated TPU, and plasma pretreated TPU (without LIT). The samples were exposed to 95 ± 2% relative humidity (RH) at varying temperatures (60 °C for 2 days, 50 °C for 3 days, and 40 °C for 5 days) in an environmental chamber to simulate accelerated degradation. The chamber was cycled on and off daily, introducing repeated humid/dry and thermal fluctuations. The results, summarized in Figure S8, highlighted the superior performance of LIT-based interfaces. MXenes/glass and MXenes/TPU exhibited no delamination throughout the entire experiment, maintaining values below ∼40 Ω/sq for MXenes/glass and 10 Ω/sq for MXenes/TPU. Thus, despite significant surface inhomogeneity of the porous structure, the measured sheet resistance values remain acceptable for the device operation even under aggressive environmental conditions.

In contrast, nonprocessed control samples degraded rapidly; for MXenes on TPU without LIT, the sheet resistance increased to ∼1 kΩ/sq, while MXenes on glass underwent complete delamination. These results highlight the effectiveness of laser sintering in prolonging MXene functionality under extreme conditions. Notably, plasma pretreatment of TPU substrates maintained high conductivity, even under harsh conditions, as evident in both LIT MXenes/TPU samples and plasma pretreated references (without LIT). Thus, we propose using LIT as a complementary approach to plasma pretreatment, particularly for applications requiring resilient interfaces (Figure S8).

The second test was focused on our target MXenes/glass and MXenes/TPU interfaces (without plasma pretreatment). Samples were continuously aged for 1 week at 95 ± 2% RH and ∼40 °C, with sheet resistance measured initially and again after 1, 4, and 6 days. To accelerate degradation further, the samples were also immersed in boiling water overnight. Figure 5a summarizes the sheet resistance changes under high humidity for all samples.

In this test, we conducted statistical analysis on multiple MXenes/glass and MXenes/TPU interfaces fabricated using two different laser pulse energies (LPE): 350 mJ/pulse with 7 pulses (LPE 1) and 380 mJ/pulse with 11 pulses (LPE 2), with the laser spot size of ∼200 × 50 μm. The results are summarized in Table 1.

The sheet resistance of freshly fabricated MXenes/glass interfaces was similar or slightly higher than that of pristine MXenes (0.9 ± 0.1 Ω/sq). After 6 days of the experiment, there is a distinguishable degradation in electrical properties of all samples (Table 1), which indicates incomplete suppression

https://doi.org/10.1021/acsami.5c18259
ACS Appl. Mater. Interfaces XXXX, XXX, XXX−XXX

Table 1. Changes in Electrical Properties of MXenes/Glass and MXenes/TPU Interfaces upon Aging

Configuration	Before aging (Ω/sq)	After aging (Ω/sq)
MXenes/glass (LPE 1)	4.4 ± 1.1	17.9 ± 5.9
MXenes/glass (LPE 2)	4.3 ± 2.1	17.8 ± 8.3
MXenes/TPU (LPE 1)	13.1 ± 6.6	189.2 ± 66.4
MXenes/TPU (LPE 2)	9.6 ± 9.5	22.8 ± 8.9

of oxidation, as also confirmed by XPS (Table S1, Figure S9). The trends for the best-performing interfaces among the investigated ones are shown in Figure S10. The degradation of electrical properties was more significant for the MXenes/TPU interface (Table 1), especially for LPE 1, likely due to the lower MXene content and greater surface roughness compared to the glass interface, which also contributed to the variability in sheet resistance. However, XPS showed that the overall C/O ratio for MXenes/TPU after aging remained higher than for MXenes/glass (Table S1), likely due to the influence of the polymer substrate. These results align closely with the initial test for MXenes/glass interfaces (17.3 ± 2.4 Ω/sq after 10 days of testing), while MXenes/TPU showed greater variability (6.1 ± 3.3 Ω/sq at the end of the first test). This indicates that LIBT offers more consistent results than LIFT. Achieving stable values for MXenes/TPU requires additional optimization and follow-up work, while plasma pretreatment appears preferable for this case.

Crucially, for the second test, MXenes remained firmly attached to the substrates, showing no visual signs of degradation or delamination. Optical microscopy on day 3 revealed no significant surface changes. The choice of the laser parameters was critical; for instance using an IR laser, which is the most common wavelength in laser processing, resulted in complete degradation after 1 day of exposure to identical humidity and temperature conditions in the environmental chamber. While the blue laser leads to interfacial bonding without structural decomposition, the IR laser (10.6 μm) induces structural damage, likely due to excessive heat (Figure S11). To better demonstrate enhanced adhesion, we performed cross-cut tests on the representative interfaces, following the ASTM D3359 standard. Our results show that MXenes/glass interfaces achieved a 4B rating (less than 5% of the coating removed), while pristine MXenes detached entirely from polymer surfaces (Figure S1). MXenes deposited on plasma pretreated TPU substrates fell into the 1B category (35−65% removed). Thus, the LIT approach to nonplasma-treated surfaces offers advantages for long-term mechanical stability. A detailed comparison of all results is presented in Table S3.

Moreover, environmental and adhesion tests indicate that plasma pretreatment enhances the performance of MXenes/TPU under harsh conditions. However, in scenarios involving mechanical interventions, plasma pretreatment is not as effective as LIT interfaces, which provide better adhesion and greater resistance to delamination.

In summary, average sheet resistance values after the tests remained below 25 Ω/sq throughout the aging process for MXenes/glass, and below 95 Ω/sq for MXenes/TPU, indicating robust interfaces. Notably, after the chamber, Raman spectra confirmed the presence of MXenes- and carbon-related peaks, as observed before exposure, while the original free-standing MXenes showed significant oxidation (Figure S12).

Our method offers significant improvements in the stability and substrate adherence of MXene composites, contrasting with previous reports on laser-based approaches for MXene composites, such as microbubble printing,[4] which reported a performance loss of over 85% after 62 days of air exposure. Our LIT-engineered interfaces retained a low sheet resistance (<25 Ω/sq) under harsh aging conditions. Additionally, LIT offers competitive advantages over standard methods for stabilizing MXenes, simultaneously addressing both adhesion and oxidation issues. In contrast, most conventional methods resolve only one of these challenges (Table S4).

2.5. MXenes/Glass Applications: Electrothermal Heater. Electrically driven heaters are increasingly popular for applications such as smart windows, antifogging, and eco-friendly construction materials, or as components for electrothermal actuators. These devices are often based on graphene or carbon nanotubes because of their excellent electrothermal properties.[33] Here, we explored MXenes/glass for this purpose (Figure 5b). The device's initial resistance was 4.7 Ω and remained remarkably stable. Our interfaces achieved three key performance metrics: reaching 140 °C in 45 s at a heating rate of 3.1 °C/s; maintaining stable operation at ∼100 °C for over 100 h; and exhibiting stable behavior during at least 100 heating/cooling cycles to 100 °C. Additionally, we operated the device at ∼85 °C for over 70 h. At the end of these tests, the device continued to demonstrate stable performance and homogeneous heating (Figure S13). This performance without structure degradation suggests that MXene-based heaters are a competitive alternative to graphene-based ones in various advanced applications (See comparative Table S5).

Besides the electrothermal heater, the MXenes/glass interface could be promising for memristor applications. For this purpose, we used the same MXene/glass interface employed for the electrothermal heater demonstration to evaluate memristive switching within the voltage range from −4 V to +4 V. Switching occurred at approximately ±2 V, with a low resistance state (LRS) of 10.8 Ω at +2 V and a high resistance state (HRS) of 14.1 Ω at −2 V. Although this represents only a ∼30% relative difference between states, the key observation is the device's operational reliability, maintaining stable performance over 700 cycles (see Note S4 and Figure S14). Nevertheless, this performance serves as a starting point and requires further optimization in follow-up studies.

2.6. MXenes/Polymer Applications: Breath Sensor. To demonstrate the generalizability of our LIT approach, we substituted TPU by polyethylene terephthalate (PET) as the donor substrate, while keeping all other conditions intact. While the resulting MXenes/glass interfaces were indistinguishable from those discussed earlier, showing comparable morphology, adhesion, and electrical properties, the MXenes/PET interfaces exhibited promising practical potential.

The MXenes/PET interfaces were thoroughly washed to remove loosely attached MXenes, resulting in a semi-transparent surface with a sheet resistance in the kΩ/sq range (Figure S15). The MXenes/PET interface demonstrated remarkable performance as a breath sensor (Figure 5c), exhibiting an instantaneous resistance change of approximately 300% upon exposure to human breath. This high sensitivity arises from the layered structure of MXenes and their abundant surface functional groups, which readily interact with moisture in exhaled breath. Water vapor adsorption causes interlayer swelling, which increases the resistance values.[34] Such rapid and reversible sensing opens the perspectives for this in

https://doi.org/10.1021/acsami.5c18259
ACS Appl. Mater. Interfaces XXXX, XXX, XXX−XXX

wearable health monitoring, where real-time detection of respiratory patterns or biomarkers could enable noninvasive diagnostics. Moreover, having robust but flexible MXenes-based interfaces opens the perspectives for high-performing deformation sensors and actuators.[35]

Although currently demonstrated devices have relatively small areas (several cm^2), the LIT method holds promise for scaling to larger areas for applications such as antennas and energy harvesting. Realizing this potential requires the systematic engineering of the process, including the uniform deposition of MXene films via scalable techniques such as spray, spin, or blade coating. This approach also involves investigating the impact of each MXene synthesis step on the transfer process and potentially combining it with plasma pretreatment of the substrates. Additionally, it is needed to ensure homogeneous mechanical pressure and adapt the system to industrial lasers with larger processing areas to achieve uniform and reliable large-area MXene transfer.[36] Looking ahead, the LIT approach holds promise not only for future scalability but also for broadening the scope of functional devices by integrating LIT-processed MXenes with complementary nanomaterials. For instance, hybridizing MXenes with nanoparticles, nanowires, liquid metals, or emerging structures like metal−organic frameworks and perovskites could unlock synergistic properties for advanced applications.[16] This could result in cutting-edge photocatalytic applications,[37] high-performing motion sensors,[38] or even soft robotics.[39]

3. CONCLUSIONS

We have developed a single-step LIT process to fabricate two MXenes/substrate interfaces with enhanced adhesion and prolonged environmental stability. This process is based on the combined mechanisms of LIBT and LIFT to transfer $Ti_3C_2T_x$ films onto glass and TPU substrates without the need for additional pre- or post-treatments. Morphological and spectroscopic characterization confirmed that the process preserves the original MXenes structure, while inducing partial CDC formation and solid-state sintering at the interfaces, especially prominent for MXenes/glass. This dual mechanism effectively minimizes further oxidation of MXenes on both substrates by creating a protective, carbon-rich interfacial layer. Consequently, it results in durable, electrically conductive surfaces (from single to tens of Ω/sq) that retain their performance under prolonged exposure to high humidity and elevated temperatures. The ability of the interfaces to endure mechanical peeling and immersion in boiling water verifies their potential for real-world devices. This practical potential was validated through the fabrication of an electrothermal heater and a breath sensor, both of which demonstrated reliable operation. This work highlights the capabilities of laser processing beyond a simple patterning or transfer technique, but as a powerful engineering strategy for advancing MXene-based electronics and sensors in real-world applications.

4. EXPERIMENTAL SECTION

4.1. $Ti_3C_2T_x$ Synthesis. $Ti_3C_2T_x$ was synthesized via chemical liquid etching of Ti_3AlC_2 (200 meshes, Forsman Co., China) using 40 wt % hydrofluoric acid (HF). The powder was immersed in the HF acid at a 1:10 ratio, stirred for 6−18 h at room temperature, and then washed until the pH >6. After vacuum filtration and freeze-drying, the multilayered powder was dispersed in DMSO and then in distilled water. Delamination was achieved through sonication and centrifugation, producing exfoliated $Ti_3C_2T_x$ flakes.

4.2. $Ti_3C_2T_x$-Film Deposition. Exfoliated $Ti_3C_2T_x$ was dispersed in water at a concentration of 30 mg/mL. The mixture underwent sonication for 2 min, followed by 60 s of centrifugation, and an additional 3 min of oscillation. The resulting dispersion was drop-casted onto a TPU substrate (0.55 ± 0.03 mm thick) at a ratio of ∼300 $\mu L/cm^2$ and dried in air. The thickness of the dry film was ∼35−40 μm, while thinner films did not result in efficient LIT. The impact of the thicker films will be investigated in follow-up work.

4.3. Plasma Pretreatment of TPU Substrate. The TPU film was treated with oxygen plasma for 60 s at a Radio Frequency power of 100 W, using a custom-built plasma system. The TPU sample was placed inside the vacuum chamber. High-purity oxygen gas was introduced and ionized into plasma under the applied high-voltage electric field. The generated oxygen plasma bombarded the TPU surface, modifying its chemical and physical properties.

4.4. Laser-Induced Transfer. A $Ti_3C_2T_x$ film on TPU was sandwiched between two glass microscope slides (1.04 ± 0.01 mm thick). The assembly was mechanically pressed along its borders to ensure uniform pressure and close contact between substrates. Irradiation was performed using a 436 nm laser. Laser parameters varied for specific experiments and are summarized in Note S2 and mentioned in the main text where applicable. The interpixel distance was ∼200 μm. The laser beam was focused through the top glass slide onto the $Ti_3C_2T_x$ film on TPU, as illustrated in Figure 1. Irradiation time depends heavily on the desired geometry; for most representative samples in this work (approximately 2 cm × 1 cm in size), it was approximately 2.5 min. For smaller areas, irradiation takes less than a minute. After irradiation, the top glass was carefully removed. MXenes adhered to this glass via LIBT, forming MXenes/glass, while MXenes remaining on TPU formed MXenes/TPU through LIFT.

4.5. XPS. The XPS spectra were recorded using a Thermo Fisher Scientific XPS NEXSA spectrometer, equipped with an Al Kα X-ray monochromatic emitter with an energy of 1486.6 eV. Survey spectra were recorded using radiation with an energy of 200 eV and an energy resolution of 1 eV. High-resolution spectra were collected using radiation with an energy of 50 eV and a resolution of 0.1 eV. The analysis area was 400 μm. A flood gun was used to compensate for the charges. A monatomic gun was used for depth profiling with an energy of 3800 eV. For each spectrum, two different areas were recorded.

4.6. SEM-EDX. The morphology of our materials was characterized using a SU8220 FESEM (Hitachi, Ltd., Japan) with a resolution of higher than 0.8 nm at an accelerating voltage of 15 kV. Cross-sectional EDX mapping was performed with a Magellan 400 FESEM (Thermo Fisher Scientific). To prepare sharp cross sections, MXene films and interfaces were placed into liquid nitrogen and then fractured using tweezers. The resulting fragments were put on a vertical holder and loaded into the microscope chamber.

Additionally, SEM images were recorded using COXEM EM-30 PLUS at an accelerating voltage of 15 kV.

4.7. Optical Images. Surface morphology was evaluated using Micromed 3LUM microscope (transmittance mode) and NTEGRA Spectra, NT-MDT Raman system (reflectance mode).

4.8. Raman Spectroscopy. A Raman spectrometer (NTEGRA Spectra, NT-MDT, Russia) equipped with an electron-multiplying charge-coupled detector (Andor Newton, UK) cooled to − 65 °C was employed for the Raman measurements. A diode laser system emitting at 532 nm wavelength, a 600 lines/mm grating, and a 20x objective were used for recording the Raman spectra. The calibration was performed using the sharp peak of Si at 520.7 cm^{-1}. For Raman mapping, the acquisition time was set to 0.1 s, capturing an image size of 5 × 5 μm^2 to obtain reproducible spectra.

4.9. XRD. XRD patterns were obtained using two setups: 1) D8 DISCOVER DAVINCI (BRUKER AXS GmbH, Germany). The sample was wholly fixed on the sample stage and scanned by a microfocus X-ray beam. The double diffraction angle (2θ) ranged

https://doi.org/10.1021/acsami.5c18259
ACS Appl. Mater. Interfaces XXXX, XXX, XXX−XXX

from 5° to 80°. And 2) XRD-7000S diffractometer (Shimadzu, Kyoto, Japan).

4.10. Sheet Resistance. MST 4000A microprobe station (MS Tech Korea Co Ltd., South Korea) was used to position the tips in a square configuration. Electrical characterization was performed on the potentiostat-galvanostat P-45X (Electrochemical Instruments, Russia). Sheet resistance was calculated using the following eq 1:

$$R_{(s)} = \frac{2\pi}{\ln(2)} \times \frac{\Delta V}{I} \quad (1)$$

where $R_{(s)}$: sheet resistance; ΔV: the change in voltage measured between the backside probes; I: the current applied between the inside probes.

For several measurements, we also used a portable device to measure sheet resistance.

4.11. Aging Test. We performed two tests using a custom humidity chamber capable of maintaining temperatures in the range of 30−60 °C and RH up to 98%. The chamber was placed on a controlled heating plate, with water vapor introduced via a pump to achieve the desired humidity levels. Internal conditions were monitored using an external temperature and humidity sensor hermetically sealed within the chamber.

In the first test, samples were exposed for a total of 10 days at 95% RH. The temperature varied as follows: 60 °C for 2 days, 50 °C for 3 days, and 40 °C for 5 days. The chamber was cycled on and off daily to introduce repeated environmental stresses. Samples included MXenes/glass and MXenes/TPU interfaces (with and without plasma pretreatment of TPU), as well as references (MXenes deposited directly on glass, untreated TPU, and plasma pretreated TPU without LIT).

In the second test, focused on constant conditions, samples (primarily target MXenes/glass and MXenes/TPU without plasma pretreatment) were aged continuously for 1 week at 95% RH and ∼40 °C.

For both tests, sheet resistance was measured using the four-probe method. Samples were periodically removed from the chamber and allowed to dry in ambient air before the test.

4.12. Adhesion Test. Adhesion was evaluated using the standard ASTM D3359 tape test. The sample surfaces were cross-cut using a sharp blade to create a lattice pattern with a 3 mm spacing and six parallel cuts in each direction. Pressure-sensitive adhesive tape (Type 1, Class A, complying with CID A-A-113) was applied over the cut area and firmly pressed down for 60 s to ensure full contact. The tape was then rapidly removed at an approximate 45° angle. The adhesion quality was assessed by examining the surface under an optical microscope to identify any coating removal or damage.

4.13. Electrothermal Heater. We fabricated the MXenes/glass interface with a size of ∼2 × 1 cm^2 using the same LIT approach (LPE 350 mJ/pulse). For the contacts, we utilized copper tape and silver paste.

4.14. Breath Sensor. The breath sensor was fabricated using the same sandwich structure described in the Laser-Induced Transfer subsection (LPE of 350 mJ/pulse), with the thermoplastic TPU substrate replaced by PET. No substrate pretreatment was applied; the MXene dispersion was deposited on the substrate at a ratio of ∼300 μL per cm^2. The sensor size was approximately 1 × 0.8 cm^2. MXenes/PET was thoroughly washed from the nonsintered MXenes and used as a proof-of-concept breath sensor. Current−time response curves were recorded using a P-45X potentiostat-galvanostat to demonstrate the sensor's proof-of-concept performance.

4.15. Memristor. To demonstrate memristive switching, we utilized the electrothermal heater MXenes/glass sample. The memristive switching was measured using the MST 4000A microprobe station (MS Tech Korea Co., Ltd., South Korea) in a two-probe scheme, with a potential window of up to ± 6 V.

■ ASSOCIATED CONTENT

Supporting Information

The Supporting Information is available free of charge at https://pubs.acs.org/doi/10.1021/acsami.5c18259.

Photos of the samples, laser processing in air, the selection of laser parameters, details on XPS and aging experiments, a table summarizing the adhesion evaluation of different samples, comprehensive tables comparing our work to relevant manuscripts, and possibilities of LIT interfaces for memristors, systematic study of the effect of laser parameters on LIT (PDF)

■ AUTHOR INFORMATION

Corresponding Authors

Anna Lipovka − *Tomsk Polytechnic University, Tomsk 634050, Russia;* orcid.org/0000-0002-2012-1569; Email: lipovka.a@gmail.com

Raul D. Rodriguez − *Tomsk Polytechnic University, Tomsk 634050, Russia;* orcid.org/0000-0003-4016-1469; Email: raul@tpu.ru

Ranran Wang − *The State Key Lab of High Performance Ceramics and Superfine Microstructure, Shanghai Institute of Ceramics, Chinese Academy of Sciences, Shanghai 200050, China; School of Chemistry and Materials Science, Hangzhou Institute for Advanced Study, University of Chinese Academy of Sciences, Hangzhou 310024, China;* orcid.org/0000-0001-5097-2834; Email: wangranran@mail.sic.ac.cn

Authors

Aura Garcia − *Tomsk Polytechnic University, Tomsk 634050, Russia*

Dmitry Kogolev − *Tomsk Polytechnic University, Tomsk 634050, Russia;* orcid.org/0000-0003-0809-3224

Ziyang Song − *The State Key Lab of High Performance Ceramics and Superfine Microstructure, Shanghai Institute of Ceramics, Chinese Academy of Sciences, Shanghai 200050, China*

Evgeniya Sheremet − *Tomsk Polytechnic University, Tomsk 634050, Russia;* orcid.org/0000-0003-3937-8628

Complete contact information is available at: https://pubs.acs.org/10.1021/acsami.5c18259

Author Contributions

A. Lipovka: Conceptualization, Investigation, Validation, Formal analysis, Visualization, Writing—original draft, Writing—review and editing. **R. D. Rodriguez**: Conceptualization, Investigation, Writing—review and editing. **A. Garcia**: Investigation, Writing—original draft, Writing—review and editing. **D. Kogolev**: Investigation, Validation, Writing—review and editing. **Z. Song**: Investigation, Validation, Writing—review and editing. **R. Wang**: Conceptualization, Writing—review and editing, Funding acquisition. **E. Sheremet**: Conceptualization, Writing—review and editing, Funding acquisition.

Notes

The authors declare no competing financial interest.

■ ACKNOWLEDGMENTS

This work was supported by a Russian Science Foundation Grant No. 23-42-00081 (China-Russia Collaboration project NSFC number 62261136551). Ranran Wang acknowledges the support from the National Natural Science Foundation of

China (Grant No. 62261136551). The authors are grateful to TPU's center "Physical and chemical methods of analysis" for XPS measurements. We thank Maxim Syrtanov for the help with XRD measurements.

REFERENCES

(1) Shayesteh Zeraati, A.; Mirkhani, S. A.; Sun, P.; Naguib, M.; Braun, P. V.; Sundararaj, U. Improved Synthesis of TiCT MXenes Resulting in Exceptional Electrical Conductivity, High Synthesis Yield, and Enhanced Capacitance. *Nanoscale* **2021**, *13* (6), 3572−3580.
(2) Shahzad, F.; Iqbal, A.; Kim, H.; Koo, C. M. 2D Transition Metal Carbides (MXenes): Applications as an Electrically Conducting Material. *Adv. Mater.* **2020**, *32* (51), No. e2002159.
(3) Cui, J.; Peng, Q.; Zhou, J.; Sun, Z. Strain-Tunable Electronic Structures and Optical Properties of Semiconducting MXenes. *Nanotechnology* **2019**, *30* (34), 345205.
(4) Herber, M.; Hill, E. H. Optically-Directed Bubble Printing of MXenes on Flexible Substrates toward MXene-Enabled Wearable Electronics and Strain Sensors. *Nano Lett.* **2025**, *25* (18), 7258−7265.
(5) Tan, Y.; Zhao, Y.; Chen, X.; Zhai, S.; Wang, X.; Su, L.; Yang, H.; Deng, W.-Q.; Ho, G. W.; Wu, H. Cooperative Cu with Defective MXene for Enhanced Nitrate Electroreduction to Ammonia. *EcoEnergy* **2024**, *2* (2), 258−267.
(6) Taha, M.; Agha, A.; Anwer, S.; Saleh, H.; Pappa, A.-M.; Abu-Nada, E.; Alazzam, A. Fabrication and Optimization of $Ti_3C_2T_x$ MXene Thin Films for Next-generation Lab-on-chip Devices. *Adv. Mater. Interfaces* **2025**, *12* (12). DOI: 10.1002/admi.202500205.
(7) Lee, A.; Shekhirev, M.; Anayee, M.; Gogotsi, Y. Multi-Year Study of Environmental Stability of Ti3C2Tx MXene Films. *Graphene and 2D mater* **2024**, *9* (1−2), 77−85.
(8) Naysmith, A. L. T.; Smith, T.; Mian, N. S.; Hewitt, A. The Effect of Plasma Pre-Treatment on the Electrical Resistance of MXene (Ti3C2Tx) Coated Fabrics. *Mater. Adv.* **2025**, *6*, 2278.
(9) Zhao, L.; Bi, L.; Hu, J.; Gao, G.; Zhang, D.; Li, Y.; Flynn, A.; Zhang, T.; Wang, R.; Cheng, X. M.; Liu, L.; Gogotsi, Y.; Li, B. Universal Salt-Assisted Assembly of MXene from Suspension on Polymer Substrates. *Nat. Commun.* **2024**, *15* (1), 10027.
(10) Fang, H.; Thakur, A.; Zahmatkeshsaredorahi, A.; Fang, Z.; Rad, V.; Shamsabadi, A. A.; Pereyra, C.; Soroush, M.; Rappe, A. M.; Xu, X. G.; Anasori, B.; Fakhraai, Z. Stabilizing TiCT MXene Flakes in Air by Removing Confined Water. *Proc. Natl. Acad. Sci. U. S. A.* **2024**, *121* (28), No. e2400084121.
(11) Tang, H.; Wang, R.; Shi, L.; Sheremet, E.; Rodriguez, R. D.; Sun, J. Post-Processing Strategies for Improving the Electrical and Mechanical Properties of MXenes. *Chem. Eng. J.* **2021**, *425*, 131472.
(12) Lee, S.; Kim, E. H.; Yu, S.; Kim, H.; Park, C.; Lee, S. W.; Han, H.; Jin, W.; Lee, K.; Lee, C. E.; Jang, J.; Koo, C. M.; Park, C. Polymer-Laminated TiCT MXene Electrodes for Transparent and Flexible Field-Driven Electronics. *ACS Nano* **2021**, *15* (5), 8940−8952.
(13) Manshina, A. A.; Tumkin, I. I.; Khairullina, E. M.; Mizoshiri, M.; Ostendorf, A.; Kulinich, S. A.; Makarov, S.; Kuchmizhak, A. A.; Gurevich, E. L. The Second Laser Revolution in Chemistry: Emerging Laser Technologies for Precise Fabrication of Multifunctional Nanomaterials and Nanostructures. *Adv. Funct. Mater.* **2024**, DOI: 10.1002/adfm.202405457.
(14) Han, D.-D.; Zhang, Y.-C.; Li, J.-C.; Zhou, H.; Mao, J.-W.; Zhang, Y.-L.; Sun, H.-B. A Conformal Active-Material Loading Strategy for Designing High-Performance Planar Microsupercapacitors. *IEEE Electron Device Lett.* **2023**, *44* (10), 1688−1691.
(15) Zhang, J.-R.; Li, A.; Li, X.-L.; Zhao, Y.-B.; Sun, J.-S.; Guo, X.-X.; Wang, W.; Liu, J.; Zhang, Y.-L.; Han, D.-D. High-Resolution Stretchable Soft Liquid Metal Circuits Based on Cu-Ga Alloying and Femtosecond Laser Ablation. *ACS Appl. Mater. Interfaces* **2025**, *17* (12), 18940−18953.
(16) Lipovka, A.; Garcia, A.; Abyzova, E.; Fatkullin, M.; Song, Z.; Li, Y.; Wang, R.; Rodriguez, R. D.; Sheremet, E. Laser Processing of Emerging Nanomaterials for Optoelectronics and Photocatalysis. *Adv. Opt. Mater.* **2024**, *12* (17). DOI: 10.1002/adom.202303194.
(17) Li, Y.; Yang, Z.; Chen, X.; Zhang, S.; Xu, S.; Li, P.; Yi, L.; Liu, F. Laser Thermochemical Synthesis of MXene/graphene Heterostructure for a Highly Sensitive Flexible Pressure Sensor. *ACS Appl. Electron. Mater.* **2024**, *6* (7), 5117−5125.
(18) Deshmukh, S.; Ghosh, K.; Pykal, M.; Otyepka, M.; Pumera, M. Laser-Induced MXene-Functionalized Graphene Nanoarchitectonics-Based Microsupercapacitor for Health Monitoring Application. *ACS Nano* **2023**, *17* (20), 20537−20550.
(19) Herber, M.; Hanly, B. M.; Hill, E. H. Laser-Directed Bubble Printing of MXene-Based Composites: A Simple Route to Micropatterned Photodetectors. *ACS Appl. Mater. Interfaces* **2025**, *17* (26), 38269−38279.
(20) Chen, H.; Wen, Y.; Qi, Y.; Zhao, Q.; Qu, L.; Li, C. Pristine Titanium Carbide MXene Films with Environmentally Stable Conductivity and Superior Mechanical Strength. *Adv. Funct. Mater.* **2020**, *30* (5), 1906996.
(21) Tang, J.; Yi, W.; Zhong, X.; Zhang, C.; Xiao, X.; Pan, F.; Xu, B. Laser Writing of the Restacked Titanium Carbide MXene for High Performance Supercapacitors. *Energy Storage Mater.* **2020**, *32*, 418−424.
(22) Park, S.; Choi, S. H.; Kim, J. M.; Ji, S.; Kang, S.; Yim, S.; Myung, S.; Kim, S. K.; Lee, S. S.; An, K.-S. Nanoarchitectonics of MXene Derived TiO /Graphene with Vertical Alignment for Achieving the Enhanced Supercapacitor Performance. *Small* **2024**, *20* (6), No. e2305311.
(23) Rodriguez, R. D.; Fatkullin, M.; Garcia, A.; Petrov, I.; Averkiev, A.; Lipovka, A.; Lu, L.; Shchadenko, S.; Wang, R.; Sun, J.; Li, Q.; Jia, X.; Cheng, C.; Kanoun, O.; Sheremet, E. Laser-Engineered Multifunctional Graphene-Glass Electronics. *Adv. Mater.* **2022**, *34* (43), No. e2206877.
(24) Li, Y.; Zeng, Z.; Zhang, S.; Guo, D.; Li, P.; Chen, X.; Yi, L.; Zheng, H.; Liu, S.; Liu, F. Highly Efficient Laser Bidirectional Graphene Printing: Integration of Synthesis, Transfer and Patterning. *Small* **2024**, *20* (45), No. e2404001.
(25) Safarkhani, M.; Far, B. F.; Huh, Y.; Rabiee, N. Thermally Conductive MXene. *ACS Biomater. Sci. Eng.* **2023**, *9* (12), 6516−6530.
(26) Hart, J. L.; Hantanasirisakul, K.; Lang, A. C.; Anasori, B.; Pinto, D.; Pivak, Y.; van Omme, J. T.; May, S. J.; Gogotsi, Y.; Taheri, M. L. Control of MXenes' Electronic Properties through Termination and Intercalation. *Nat. Commun.* **2019**, *10* (1), 522.
(27) Rasel, M. A. J.; Wyatt, B.; Wetherington, M.; Anasori, B.; Haque, A. Low-Temperature Annealing of 2D Ti3C2Tx MXene Films Using Electron Wind Force in Ambient Conditions. *J. Mater. Res.* **2021**, *36* (17), 3398−3406.
(28) Mukasyan, A. S.; Rogachev, A. S.; Moskovskikh, D. O.; Yermekova, Z. S. Reactive Spark Plasma Sintering of Exothermic Systems: A Critical Review. *Ceram. Int.* **2022**, *48* (3), 2988−2998.
(29) Qian, B.; Shen, Z. Laser Sintering of Ceramics. *J. Asian Ceram. Soc.* **2013**, *1* (4), 315−321.
(30) Krishnan, S.; Marimuthu, S.; Singh, M. K.; Rai, D. K. Two-Dimensional $Ti_3C_2T_x$ MXene Nanosheets for CO_2 Electroreduction in Aqueous Electrolytes. *Energy Adv.* **2023**, *2*, 1166.
(31) Sarycheva, A.; Gogotsi, Y. Raman Spectroscopy Analysis of the Structure and Surface Chemistry of $ti_3C_2T_x$ MXene. *Chem. Mater.* **2020**, *32* (8), 3480−3488.
(32) Jenila, T. J.; Infancy, W. T.; Rathikha, R.; Vinosha, P. A.; Ayyar, M.; Ramasamy, S.; Maruthasalamoorthy, S.; Navamathavan, R.; Xavier, B.; Alhuthali, A. M. S.; Abo-Dief, H. M.; Abdellattif, M. H.; Balachandran, R.; Hossain, M. K. Unraveling the Role of MXene (TiCT) Integrated Cu-Doped WO Nanocomposites via Co-Precipitation Technique for Enhanced Supercapacitor Performance. *Sci. Rep.* **2025**, *15* (1), 25007.
(33) Cui, L.; Cui, K.; Ci, H.; Zheng, K.; Xie, H.; Gao, X.; Zhang, Y.; Liu, Z. Transparent Electrothermal Heaters Based on Vertically-Oriented Graphene Glass Hybrid Materials. *Nanomaterials (Basel)* **2019**, *9* (4), 558.

https://doi.org/10.1021/acsami.5c18259
ACS Appl. Mater. Interfaces XXXX, XXX, XXX−XXX

(34) An, H.; Habib, T.; Shah, S.; Gao, H.; Patel, A.; Echols, I.; Zhao, X.; Radovic, M.; Green, M. J.; Lutkenhaus, J. L. Water Sorption in MXene/polyelectrolyte Multilayers for Ultrafast Humidity Sensing. *ACS Appl. Nano Mater.* **2019**, *2* (2), 948−955.
(35) Ma, J.-N.; Ma, B.; Wang, Z.-X.; Song, P.; Han, D.-D.; Zhang, Y.-L. Multiresponsive MXene Actuators with Asymmetric Quantum-confined Superfluidic Structures. *Adv. Funct. Mater.* **2024**, *34* (8). DOI: 10.1002/adfm.202308317.
(36) Lee, C. K. W.; Pan, Y.; Yang, R.; Kim, M.; Li, M. G. Laser-Induced Transfer of Functional Materials. *Top Curr. Chem. (Cham)* **2023**, *381* (4), 18.
(37) Han, D.-D.; Wang, Q.; Chen, Z.-D.; Wang, L.; Chang, Z.; Xie, S.-Y.; Li, X.-B.; Zhang, W.; Zhang, Y.-L. Light-Propelled Photocatalytic Evaporator for Robotic Solar-Driven Water Purification. *Photonix* **2025**, *6* (1). DOI: 10.1186/s43074-025-00169-4.
(38) Zhang, J.-R.; Li, A.; Sun, Z.-J.; Wang, Q.; Zhang, Y.-L.; Han, D.-D. High Linearity and Low Hysteresis LMPs/MXene/AgNWs Strain Sensor for Human Motion Detection. *Appl. Phys. Lett.* **2025**, *126* (3). DOI: 10.1063/5.0250361.
(39) Deng, S.; Li, Y.; Li, S.; Yuan, S.; Zhu, H.; Bai, J.; Xu, J.; Peng, L.; Li, T.; Zhang, T. A Multifunctional Flexible Sensor Based on PI-MXene/SrTiO Hybrid Aerogel for Tactile Perception. *Innovation (Camb)* **2024**, *5* (3), 100596.

https://doi.org/10.1021/acsami.5c18259
ACS Appl. Mater. Interfaces XXXX, XXX, XXX−XXX